New Lamellar Oxophosphorus Derivatives of Nickel(II): X-ray Powder Diffraction Structure Determinations and Magnetic Studies of $Ni(HPO_3)\cdot H_2O$, $NiCl(H_2PO_2)\cdot H_2O$, and $Ni_xCo_{1-x}(HPO_3)\cdot H_2O$ Solid Solutions

M. Dolores Marcos,*,†,‡ Pedro Amorós,† Fernando Sapiña,† Aurelio Beltrán-Porter,† Ramón Martínez-Máñez,§ and J. Paul Attfield‡

UIBCM, Departament de Química Inorgánica, Facultat de Química de la Universitat de València, Dr. Moliner 50, 46100-Burjassot (València), Spain, Departamento de Química de la Universidad Politécnica de Valencia, Camino de Vera s/n, 46071-Valencia, and Department of Chemistry, University of Cambridge, Lensfield Road, Cambridge CB2 1EW, U.K.

Received March 17, 1993•

The structures of the two new lamellar oxophosphorus compounds of nickel(II), $Ni(HPO_3)\cdot H_2O$ (**1**) and $NiCl(H_2PO_2)\cdot H_2O$ (**2**), have been determined by X-ray methods. The simple phosphite (**1**) crystallizes in an orthorhombic system, space group $Pca2_1$ (a = 8.8982(2) Å, b = 7.8628(2) Å, c = 10.0333(3) Å, V = 701.98(5) Å^3, Z = 4), and is isostructural with $Co(HPO_3)\cdot H_2O$. The chlorohypophosphite (**2**) also crystallizes in an orthorhombic system, space group $Pbca$ (a = 7.2986(2) Å, b = 13.0616(4) Å, c = 9.4078(3) Å, V = 896.85(7) Å^3, Z = 4), being isostructural with $CoCl(H_2PO_2)\cdot H_2O$. Both structures have been refined with the Rietveld method, using as starting models the parameters of the cobalt analogues. The final reliability factors were R_F = 7.5%, R_p = 7.4%, and R_{wp} = 9.5% for **1** and R_F = 3.5%, R_p = 7.6%, and R_{wp} = 9.7% for **2**. The layers in the structure of **1** involve *cis*-$^1_\infty[Ni_2O_8]$ zigzag chains of edge-sharing octahedra, running along the [100] direction, which are interconnected in the *ac* plane through two different phosphite bridges. In the case of **2**, the bidimensional metallic net in the *ac* plane results from the linking of $[Ni_2Cl_4O_6]$ dimers through Cl^- ions and $H_2PO_2^-$ groups. Nickel and cobalt phosphites, **1**, are mutually soluble over the whole range of compositions, giving $Ni_xCo_{1-x}(HPO_3)\cdot H_2O$ solid solutions in which the cations are randomly arranged. A magnetic study of these compounds is presented.

Introduction

Although the chemistry of transition metal derivatives of H_3PO_3 and H_3PO_2 has not been widely studied, the data available in the literature show that their stoichiometric diversity and structural richness are comparable to those occurring among the better known phosphate compounds.[1,2] Besides their basic interest, potential applications of these types of solids range from their ability to act as host matrices for intercalation chemistry to possible ionic conductivity or exchange.[3,4] Also, from the theoretical point of view, these materials constitute a new challenge to the magnetic superexchange interactions supported by low-symmetry diamagnetic anions.[5,6]

The lack of systematic investigations in the literature has made it necessary to perform thorough preparation and characterization studies to develop our work. We recently reported a synthetic approach which, by controlling two main variables (pH and metal ion concentration), allowed us to obtain a set of Co, Ni, and Zn derivatives showing different structural types.[2,7,8]

Whereas some results have been advanced in the literature concerning cobalt and zinc derivatives,[9,10] the information on nickel phosphites and hypophosphites is very limited. For example, the structures of both $Co(HPO_3)\cdot H_2O$[11] and $CoCl(H_2PO_2)\cdot H_2O$[12] have been determined from single-crystal X-ray diffraction data, and their magnetic behavior has also been studied.[12] It was the previously observed resemblance between the chemistries of the Co/H_3PO_3 and Ni/H_3PO_3 systems[7,13] that prompted us to approach the synthesis and characterization of the nickel analogues of the above cobalt derivatives.

Here, we describe the crystal structure and magnetic properties of the two new lamellar nickel compounds $Ni(HPO_3)\cdot H_2O$ and $NiCl(H_2PO_2)\cdot H_2O$ and the preparation of $Ni_xCo_{1-x}(HPO_3)\cdot H_2O$ solid solutions over the entire range of compositions.

Experimental Section

Synthesis of $Ni(HPO_3)\cdot H_2O$ (1). Although the synthesis of **1** might be carried out in a manner similar to that previously reported for $Co(HPO_3)\cdot H_2O$,[11] some procedural modifications intended to simplify it (by avoiding intermediates) and increase the yield and crystallinity of the resulting solid have been adopted. To an aqueous solution (50 mL) containing 5 g (21.0 mmol) of $NiCl_2\cdot 6H_2O$ was slowly added with stirring the stoichiometric amount of H_3PO_3 (5 mL, 50%). Then, a concentrated solution of KOH (ca. 1.4 M) was added dropwise with stirring until pH = 4. An incipient turbidity appeared while the suspension became slightly green. The mixture was placed in a steel-covered Teflon container filled to 90% of its volume and was heated over 3 days with an external temperature of 180 °C. A very fine light green polycrystalline powder

† Universitat de València.
‡ University of Cambridge.
§ Universidad Politécnica de Valencia.
• Abstract published in *Advance ACS Abstracts*, October 15, 1993.

(1) Loub, J.; Kratochvill, B. *Chem. Listy* **1987**, *81*, 337.
(2) Marcos, M. D.; Amorós, P.; Beltrán, A.; Beltrán, D. *Solid State Ionics* **1993**, *63–65*, 96.
(3) Clearfield, A. *Chem. Rev.* **1988**, *88*, 125.
(4) Cao, G.; Hong, H.; Mallouk, T. E. *Acc. Chem. Res.* **1992**, *25*, 420.
(5) Charron, F. F.; Reiff, W. M. *J. Solid State Chem.* **1985**, *58*, 38.
(6) Villeneuve, G.; Suh, K. S.; Amorós, P.; Casañ-Pastor, N.; Beltrán, D. *Chem. Mater.* **1992**, *4*, 108.
(7) Marcos, M. D.; Amorós, P.; Beltrán, A.; Martínez-Mañez, R.; Attfield, J. P. *Chem. Mater.* **1993**, *5*, 121.
(8) Marcos, M. D.; Amorós, P.; Beltrán, D. *Solid State Ionics* **1993**, *63–65*, 87.
(9) Weakley, T. J. R. *Acta Crystallogr., B* **1979**, *25*, 42.
(10) Ortíz, C. Y.; Squattrito, P. J.; Shieh, M.; Clearfield, A. *Inorg. Chem.* **1989**, *28*, 2608.
(11) Sapiña, F.; Gómez, P.; Marcos, M. D.; Amorós, P.; Ibáñez, R.; Beltrán, D.; Navarro, R.; Rillo, C.; Lera, F. *Eur. J. Solid State Inorg. Chem.* **1989**, *26*, 603.
(12) Marcos, M. D.; Ibáñez, R.; Amorós, P.; Le Bail, A. *Acta Crystallogr., C* **1991**, *47*, 1152.
(13) Baes, C. F., Jr.; Mesmer, R. E. *The Hydrolysis of Cations*; John Wiley & Sons: New York, 1976.

0020-1669/93/1332-5044$04.00/0

Table I. Compositions and Refined Cell Parameters of the $Ni_xCo_{1-x}(HPO_3)\cdot H_2O$ Solid Solutions[a]

x (x_0)	a (Å)	b (Å)	c (Å)	V (Å^3)
1.0 (1.0)	8.884(6)	7.848(3)	10.014(6)	698.2(4)
0.71 (0.8)	8.905(1)	7.8610(5)	10.055(1)	703.9(2)
0.51 (0.6)	8.939(2)	7.8648(2)	10.075(2)	708.3(2)
0.40 (0.5)	8.930(2)	7.8688(6)	10.088(2)	708.9(3)
0.31 (0.4)	8.940(1)	7.8782(6)	10.104(2)	711.6(2)
0.12 (0.2)	8.955(2)	7.8855(1)	10.122(2)	714.8(2)
0.00 (0.0)	8.965(2)	7.8902(4)	10.150(2)	717.9(2)
Δ_i (%)	0.91(14)	0.54(4)	1.35(19)	

[a] x = found nickel molar ratio; x_0 = nickel molar ratio in the initial mother solution. Δ_i = maximum relative difference between the cell parameters (CP); $\Delta_i = (CP_0 - CP_1)/CP_1 \times 100$ (CP_0 = cell parameters of $Co(HPO_3)\cdot H_2O$; CP_1 = cell parameters of $Ni(HPO_3)\cdot H_2O$.

was separated from the mother liquor by filtration, washed with water and acetone, and air-dried. Anal.: Ni, found 37.12, calc 37.47; P, found 20.10, calc 19.77.

Synthesis of $NiCl(H_2PO_2)\cdot H_2O$ (2). The synthesis was performed by following a procedure similar to that previously reported for $CoCl(H_2PO_2)\cdot H_2O$.[12] **2** was prepared by adding 5 mL of H_3PO_2 (aqueous, 30%) to a solution containing 11.27 g (47.4 mmol) of $NiCl_2\cdot 6H_2O$ in 5 mL of distilled water. The resulting green solution was kept over sulfuric acid in a thermostated desiccator (298 K) for several weeks. Instead of the well-formed crystals obtained in the case of the cobalt compound, the resulting product was now isolated (after filtration, water and acetone washing, and air-drying) as a pale green polycrystalline solid, with a typical yield of 80%. Anal.: Ni, found 32.96, calc 33.14; P, found 17.61, calc 17.49.

Synthesis of $Ni_xCo_{1-x}(HPO_3)\cdot H_2O$ Solid Solutions (x = 0.12, 0.31, 0.40, 0.51, 0.71). Once it had been verified that the experimental procedure described above for **1** allowed us an equally advantageous preparation of the cobalt derivative, $Co(HPO_3)\cdot H_2O$, the synthesis of $Ni_xCo_{1-x}(HPO_3)\cdot H_2O$ solid solution phases was achieved by using the same procedure and starting from aqueous solutions containing the nominal stoichiometric Ni/Co ratios summarized in Table I. These preparations typically gave 80–90% of the theoretical yield.

Physical Measurements. Co, Ni, and P contents were determined, after dissolution of the solids in boiling concentrated hydrochloric acid, by atomic absorption spectrometry (Perkin-Elmer Zeeman 5000). Water was determined thermogravimetrically (Perkin-Elmer thermogravimetric analyzer TGA-7).

X-ray powder diffraction patterns were obtained from a Siemens D501 automated diffractometer using graphite-monochromated Cu Kα radiation. The diffractometer is equipped with a variable-temperature device working from room temperature to ca. 1000 °C. Patterns used for indexation were recorded with $Pb(NO_3)_2$ (analytical quality) as an internal standard and scanned in steps of 0.02° 2θ over the angular range 10–70° 2θ for 10 s/step. The TREOR program[14] was used to index the patterns. For Rietveld analysis, patterns were collected with the same scanning step (0.02° 2θ), but a wider 2θ range (10–120° 2θ) and a longer acquisition time (20 s/step) were used to enhance statistics. In order to minimize preferred orientation effects, the sample holder described by MacMurdie[15] was used. Rietveld profile analyses[16] were performed with the GSAS program[17] using a pseudo-Voigt peak shape function, corrected for asymmetry at low angles, and a refined background function.

IR spectra (KBr pellets) were recorded on a FTIR Perkin-Elmer 1750 spectrophotometer. Room-temperature (25.0 ± 0.1 °C) diffuse reflectance spectra were recorded (8000–30000 cm^{-1}) using a Perkin-Elmer Lambda-9 UV/vis/near-IR spectrophotometer.

Magnetic measurements were performed on powdered samples using an ac susceptomer, Lake Shore Cryotronics Inc. 7000 AC model, in the temperature range 4.5–130 K. The frequency and exciting field amplitude used were 133.3 Hz and 2 Oe. Both the in-phase, χ', and out-of-phase, χ'', components of the ac susceptibility were recorded. (Experimental susceptibilities were corrected for the diamagnetic contributions.[18])

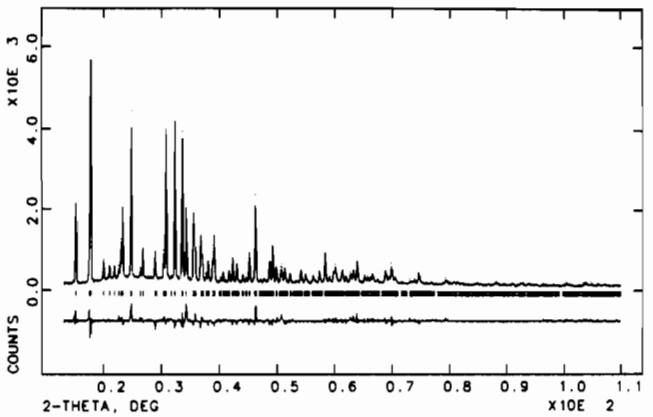

Figure 1. Observed and calculated X-ray powder diffraction patterns of $Ni(HPO_3)\cdot H_2O$. The difference is on the same scale.

Table II. Final Profile and Structural Parameters for $Ni(HPO_3)\cdot H_2O$ in Space Group $Pca2_1$

Cell Data

a = 8.8982(2) Å, V = 701.98(5) Å^3
b = 7.8628(2) Å, Z = 4
c = 10.0333(3) Å

Reliability Factors (%)

R_{wp} = 9.5 R_p = 7.4 R_F = 7.5

Structural Parameters

atom	x/a	y/b	z/c	10^2U_{iso} (Å^2)
Ni(1)	0.0998(10)	0.1290(11)	0.0800	3.28(8)
Ni(2)	–0.0940(11)	–0.1300(11)	–0.0646(4)	3.28(8)
P(1)	0.2414(13)	–0.2288(9)	–0.0188(11)	4.5(2)
P(2)	0.0857(7)	0.1257(7)	–0.2398(13)	4.5(2)
OW(1)	0.052(2)	0.385(2)	0.117(2)	1.6(3)
OW(2)	–0.071(2)	–0.388(2)	–0.119(2)	1.6(3)
O(1)	0.1043(14)	–0.1364(17)	0.0373(17)	3.2(2)
O(2)	0.2671(19)	–0.3992(12)	0.0504(12)	3.2(2)
O(3)	–0.1124(14)	0.1283(17)	–0.0028(16)	3.2(2)
O(4)	0.1843(15)	0.148(2)	–0.1178(9)	3.2(2)
O(5)	0.3217(14)	0.155(3)	0.1353(11)	3.2(2)
O(6)	0.0011(14)	0.0427(9)	0.2582(12)	3.2(2)

Structure Refinement of 1. The X-ray powder pattern of **1** was indexed from 16 accurately measured, unambiguous reflection positions. A primitive orthorhombic cell was obtained with the following parameters: a = 8.888(15) Å, b = 7.848(4) Å, and c = 10.009(8) Å (figures of merit: $M_{15} = 13$[19] and $F_{15} = 15$ (0.021, 49)[20]). This cell was very close to that reported for $Co(HPO_3)\cdot H_2O$.[11] The systematic absences were consistent with the space group of the cobalt compound, $Pca2_1$. Therefore, the determination of the structure of the nickel derivative was undertaken by starting from the structural parameters of $Co(HPO_3)\cdot H_2O$.[11]

Using this structural model for all the non-hydrogen atoms, the conventional reliability factors dropped by successive refinement cycles to R_{wp} = 13.6% and R_p = 12.2%. The refinement of the polynomial background function proved unable to reproduce the hump due to the vitreous sample holder between 14 and 35° 2θ, so a manual subtraction of all the background was made. Also the first peak in the diffractogram (001 reflection) was eliminated because of a very large asymmetry. A Fourier difference map did not enable us to find the hydrogen atoms; therefore their positions were calculated from those in the isostructural cobalt compound. An attempt to refine these hydrogen positions was unsuccessful. The final refinements were carried out with soft constraints on the Ni–O and P–O distances, allowing then to vary around the literature values for these type of bonds (2.1 Å for Ni–O and 1.52 Å for P–O distances). The final reliability factors obtained were R_{wp} = 9.46%, R_p = 7.40%, and R_F = 7.53%. Details of the final refinement and atomic parameters are given in Table II, and selected bond lengths and angles are listed in Table III. Figure 1 shows the observed and calculated patterns.

Structure Refinement of 2. The X-ray powder diffraction pattern of **2** was indexed from 20 accurately measured reflection positions. A primitive orthorhombic cell was obtained with a = 7.268(1) Å, b = 13.002-

(14) Werner, P. E. *Z. Kristallogr.* **1969**, *120*, 375.
(15) MacMurdie, H. F.; Morris, M. C.; Evans, E. H.; Paretzin, B.; Wong, W.; Hubbard, C. R. *Powder Diffr.* **1986**, *1*, 40.
(16) Rietveld, H. M. *J. Appl. Crystallogr.* **1969**, *2*, 65.
(17) Larson, A. C.; Von Dreele, R. B. Report LA-UR-86-748; Los Alamos National Laboratory: Los Alamos, NM, 1987.
(18) Earnshaw, A. *Introduction to Magnetochemistry*; Academic Press: London and New York, 1968.
(19) de Wolf, P. M. *J. Appl. Crystallogr.* **1968**, *1*, 108.
(20) Smith, G. S.; Snyder, R. L. *J. Appl. Crystallogr.* **1979**, *12*, 60.

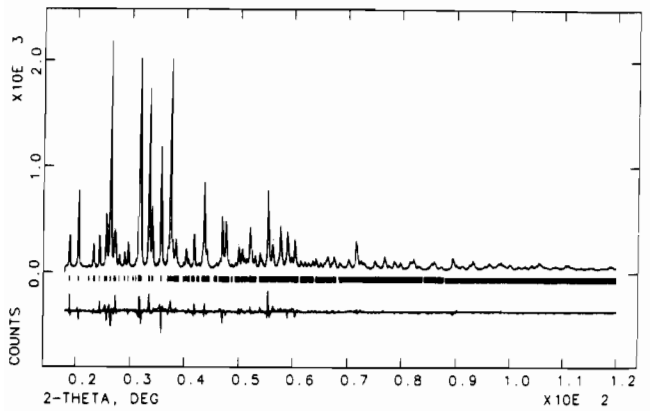

Figure 2. Observed and calculated X-ray powder diffraction patterns of $NiCl(H_2PO_2)\cdot H_2O$. The difference is on the same scale.

Table III. Bond Distances and Angles for $Ni(HPO_3)\cdot H_2O$

Ni(1)O6 Octahedron

Ni(1)	OW(1)	O(1)	O(3)	O(4)	O(5)	O(6)
OW(1)	**2.092(19)**	4.205(22)	2.770(24)	3.228(25)	3.012(26)	3.075(20)
O(1)	169.3(7)	**2.131(16)**	2.866(16)	2.818(22)	3.154(21)	2.782(19)
O(3)	83.6(7)	86.2(5)	**2.063(15)**	2.886(18)	4.109(18)	2.886(20)
O(4)	99.8(7)	82.9(5)	87.0(5)	**2.128(15)**	2.819(15)	4.193(16)
O(5)	93.0(7)	97.6(5)	170.3(5)	84.6(5)	**2.061(15)**	3.230(18)
O(6)	94.2(7)	82.1(5)	87.7(5)	164.4(5)	101.7(5)	**2.104(13)**

Ni(2)O6 Octahedron

Ni(2)	OW(2)	O(1)	O(3)	O(4)	O(5)	O(6)
OW(2)	**2.109(18)**	2.967(24)	4.238(21)	2.877(26)	3.281(24)	3.047(19)
O(1)	91.3(7)	**2.040(16)**	2.86(18)	4.049(18)	2.704(18)	3.044(20)
O(3)	177.7(7)	86.8(6)	**2.130(16)**	3.055(21)	2.686(22)	2.922(19)
O(4)	87.6(8)	164.1(6)	94.0(6)	**2.049(16)**	2.819(15)	3.174(18)
O(5)	100.8(7)	80.3(6)	77.8(6)	84.3(5)	**2.150(12)**	4.192(17)
O(6)	93.4(7)	95.3(6)	88.0(5)	100.6(5)	165.2(6)	**2.077(13)**

P(1)O3H Tetrahedron

P(1)	O(1)	O(2)	O(3)	H(1)
O(1)	**1.527(17)**	2.527(18)	2.554(18)	2.30(3)
O(2)	111.7(9)	**1.526(13)**	2.444(18)	2.30(3)
O(3)	113.2(9)	106.2(9)	**1.531(17)**	2.30(3)
H(1)	108.5(14)	108.5(12)	108.5(15)	**1.30(3)**

P(2)O3H Tetrahedron

P(2)	O(4)	O(5)	O(6)	H(2)
O(4)	**1.517(16)**	2.478(14)	2.554(19)	2.262(27)
O(5)	109.6(8)	**1.517(16)**	2.546(19)	2.263(27)
O(6)	113.8(9)	113.2(9)	**1.533(11)**	2.276(29)
H(2)	106.6(14)	106.6(14)	106.6(12)	**1.30(3)**

Short Intermetallic distances

Ni(1)-Ni(2)	3.037(11)	3.087(11)	3.566(4)

Intralayer Hydrogen Bonding Network

OW(1)-O(2)	2.64(2)	OW(1)-OW(2)	2.65(3)
OW(1)-O(2)	2.63(3)	OW(2)-O(2)	2.78(2)
OW(1)-O(3)	2.77(2)	OW(2)-O(4)	2.88(3)

(2) Å, and c = 9.352(3) Å (figures of merit: M_{20} = 32,[19] F_{20} = 50 (0.0078, 52)[20]). This cell is very similar to that of $CoCl(H_2PO_2)\cdot H_2O$, and no additional systematic absences from the expected ones for the corresponding space group (*Pbca*) were observed. The profile was fitted using the cobalt hypophosphite structure as a starting model in space group *Pbca*.

The Rietveld refinement of the framework (without hydrogen atoms) converged successfully, giving the reliability factors R_{wp} = 10.7% and R_p = 8.3%. The hydrogen positions were calculated by considering ideal C_{2v} geometries for $H_2PO_2^-$ anions and water molecules. It was not possible to refine the positions of the hydrogen atoms of the hypophosphite anions, so they were fixed at their ideal values. For the water molecule, the positions of the hydrogen atoms were refined with soft constraints on the O–H distances. Anisotropic refinement of the thermal parameters for cobalt, phosphorus, and chlorine atoms proved possible, giving the final reliability factors R_F = 3.5%, R_p = 7.6%, and R_{wp} = 9.7%. Details of the final refinement and atomic parameters are given in Table IV, and selected bond lengths and angles are listed in Table V. Figure 2 shows the observed and calculated patterns.

Cell Parameter Calculations for $Co_{1-x}Ni_x(HPO_3)\cdot H_2O$. The X-ray powder diffraction patterns were initially indexed using the TREOR program from unambiguously measured reflection positions, corrected for zero displacement with an internal standard. A primitive orthorhombic cell was obtained in all cases. Afterward, a refinement of these cell parameters with the LSUCRIPC[21] program was made, obtaining complete indexations of the diffractograms. No systematic absences apart from those expected for the $Pca2_1$ space group were observed. The refined cell parameters are shown in Table I.

Table IV. Final Profile and Structural Parameters for $NiCl(H_2PO_2)\cdot H_2O$ in Space Group *Pbca*

Cell Data

a = 7.2986(2) Å, b = 13.0616(4) Å, c = 9.4078(3) Å; V = 896.85(7) Å^3, Z = 4

Reliability Factors (%)

R_{wp} = 9.8 R_p = 7.7 R_F = 3.6

Structural Parameters

atom	x/a	y/b	z/c	10^2U_{iso} (Å^2)
Ni	0.1196(2)	0.5012(2)	0.1449(2)	1.7(1)
P	0.2254(5)	0.1530(3)	0.3884(3)	2.1(2)
Cl	0.8750(4)	0.3993(2)	0.2623(3)	1.2(2)
O(1)	0.0781(9)	0.0904(5)	0.4672(8)	0.9(3)
O(2)	0.6929(11)	0.1006(8)	0.4587(7)	2.2(3)
O(3)	0.3755(10)	0.0978(6)	0.3155(7)	2.1(2)
H(1)	0.2850	0.2110	0.4780	3.5
H(2)	0.1370	0.2120	0.3060	3.5
H(3)	0.571(4)	0.097(7)	0.435(8)	3.5
H(4)	0.696(10)	0.088(6)	0.554(2)	3.5

	10^2U_{11}	10^2U_{22}	10^2U_{33}	10^2U_{12}	10^2U_{13}	10^2U_{23}
Ni	0.8(1)	2.3(2)	2.0(1)	–0.1(2)	–0.6(1)	–0.4(1)
P	3.0(2)	1.2(2)	2.0(3)	1.4(2)	–0.2(2)	–1.4(3)
Cl	1.6(2)	0.6(2)	1.5(2)	0.7(3)	–0.4(2)	–0.6(2)

Table V. Bond Distances and Angles for $NiCl(H_2PO_2)\cdot H_2O$

NiO4Cl2 Octahedron

Ni	O(3)	O(1)	O(2)	O(1)	Cl	Cl
O(3)	**2.043(7)**	4.111(2)	2.904(10)	3.045(9)	3.258(7)	3.208(8)
O(1)	172.1(2)	**2.078(7)**	3.083(11)	2.695(10)	3.341(7)	3.154(7)
O(2)	88.4(7)	94.4(6)	**2.123(9)**	2.816(10)	3.249(10)	4.605(6)
O(1)	93.6(6)	79.6(7)	82.8(7)	**2.134(7)**	4.568(5)	3.322(7)
Cl	92.5(4)	94.8(4)	90.2(5)	170.6(3)	**2.450(3)**	3.657(4)
Cl	89.6(4)	86.9(4)	173.9(3)	91.6(4)	95.6(2)	**2.488(3)**

PH2O2 Tetrahedron

P	H(1)	H(2)	O(3)	O(1)
H(1)	**1.214**	1.946	2.226(4)	2.184(6)
H(2)	103.2	**1.269**	2.294(7)	2.237(5)
O(3)	111.1(5)	112.9(6)	**1.480(6)**	2.599(9)
O(1)	104.3(6)	105.2(5)	118.8(7)	**1.541(9)**

Water molecule

O(2)-H(3)	0.92(4)	H(3)-H(4)	1.45(1)
O(2)-H(4)	0.91(4)	H(3)-O(2)-H(4)	104.7(9)

Intralayer Hydrogen Bonding Network

O(2)-H(3)···O(3)	1.82(5)	O(2)···O(3)	2.68(1)
O(2)-H(4)···Cl	2.36(6)	O(2)···Cl	3.155(9)

Interlayer Hydrogen Bonding Network

H(1)-O(2)	2.62(8)	H(2)-Cl	3.07(10)
		H(2)-Cl	3.13(10)

Results and Discussion

Synthesis. As mentioned above, in a previous work[2] we have advanced a synthetic approach intended to rationalize the obtention of transition metal derivatives of phosphorus oxoacids. The key idea in this approach is that, besides the redox and acid–base reactions owing to the anions, there are the hydrolytic processes that the metal cations may undergo in the mother solution which determine the nature of the resulting solid. As far as these processes may be regulated by controlling two main variables, pH and metal ion concentration (C_M), it would be

(21) Appleman, D. E.; Evans, H. T. Lsucre, Indexing and Least Square Refinement of Powder Data. Document No. PB-216188; NTIS: Springfield, VA.

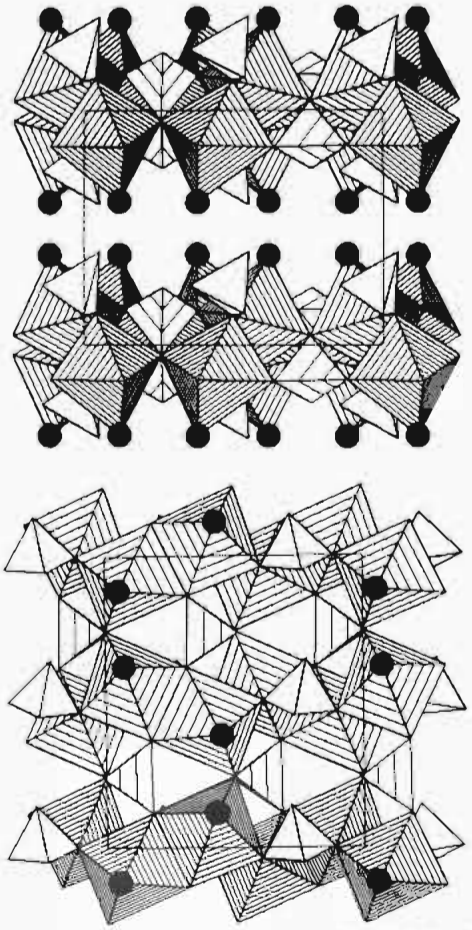

Figure 3. Projections of the crystal structure of $Ni(HPO_3)\cdot H_2O$ along the (top) [100] and (bottom) [010] directions. Circles correspond to the oxygen atoms of water molecules.

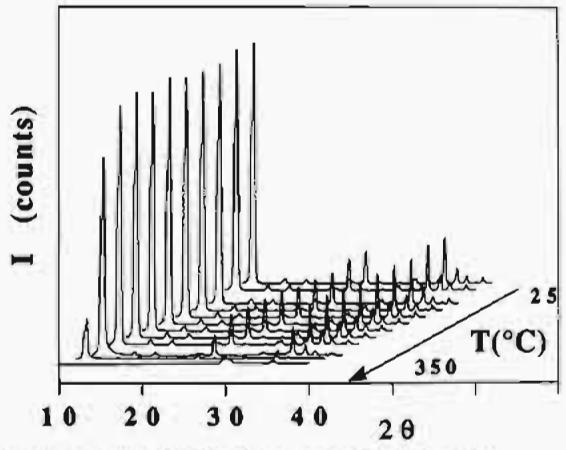

Figure 4. X-ray thermodiffractometry of $Ni(HPO_3)\cdot H_2O$.

possible to construct a given metallic framework by adjusting these variables at the appropriate point of the stability diagram. The syntheses described in the present work fit in well with hypothesis.

Thus, as discussed later, the structure of **1** involves chains of edge-shared metallic octahedra, but there were no oxo groups shared between nickel atoms. Both intrachain and interchain links are established through phosphite anions. An acid pH and relatively low metallic concentrations[13] prevent the formation in solution of the highly condensed metallic aggregates found in the $M_{11}(HPO_3)_8(OH)_6$ (M = Co, Ni, Zn) microporous materials previously described.[7,22] In the same way, the subsequent soft hydrothermal treatment (besides enhancing the crystallinity of

(22) Marcos, M. D.; Amorós, P.; Le Bail, A. *J. Solid State Chem.*, in press.

Table VI. Bond Valence Analysis for $Ni(HPO_3)\cdot H_2O$

	Ni(2)	Ni(2)	P(1)	P(2)	Σ
OW(1)	0.31(3)				0.31(3)[a]
O(1)	0.28(3)	0.35(3)	1.23(2)		1.86(8)
O(2)			1.23(2)		1.23(2)
O(3)	0.33(3)	0.28(3)	1.22(2)		1.83(8)
O(4)	0.29(3)	0.34(3)		1.27(2)	1.90(8)
O(5)	0.33(3)	0.26(3)		1.27(2)	1.86(8)
O(6)	0.30(3)	0.32(3)		1.21(2)	1.83(8)
OW(2)		0.29(3)			0.29(3)[a]
Σ	1.84(18)	1.84(18)	3.68(6)	3.75(6)	

[a] The O–H bonds of water molecules have not been included in the calculations.

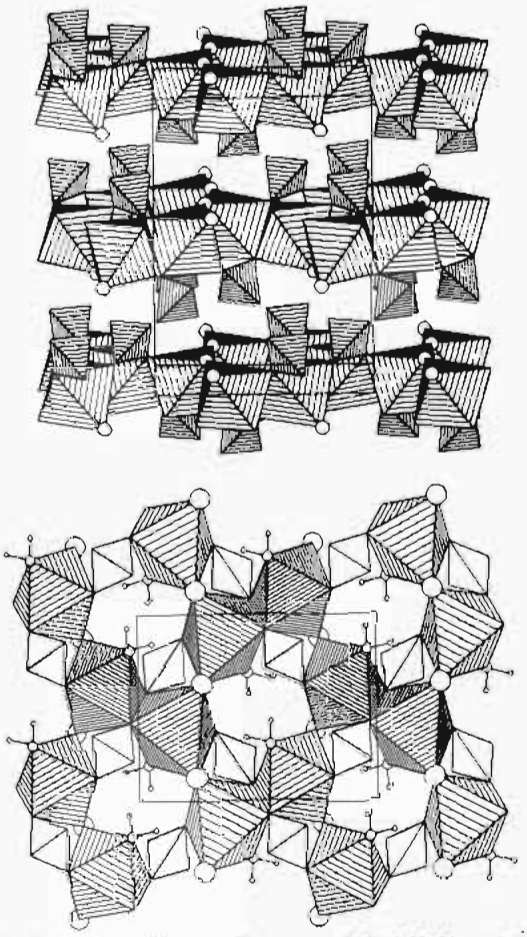

Figure 5. Projections of the crystal structure of $NiCl(H_2PO_2)\cdot H_2O$ along the (top) [100] and (bottom) [010] directions. Large circles correspond to chloride anions, and in the bottom diagram, the water molecules are shown.

the final product) results in the elimination of coordinated water molecules with a subsequent increase in the polyhedra connectivity, giving rise to the layers present in this solid. In fact, if this synthesis is performed at room *p* and *T* conditions, highly-hydrated, near-amorphous powders result.

The experimental conditions under which **2** has been obtained deserve further comments. The low coordinating ability of the hypophosphite anion when compared to phosphite or phosphate has required us to synthesize **2** at a very high Ni(II) concentration. Although this concentration is greater than those required for the synthesis of other highly condensed phases,[7] the low pH prevents the hydrolytic condensation of cation polyhedra. Hence, the condensation of the cation polyhedra should be due only to the high concentration of the reactants and should result in the formation of μ-(O)-hypophosphite bridges (corner or edge sharing among the polyhedra).[2] However, the high concentrations of Ni^{2+} required to precipitate this salt are accompanied by a high chloride ion concentration. Despite a limited coordinating tendency, chloride anions enter the nickel coordination sphere

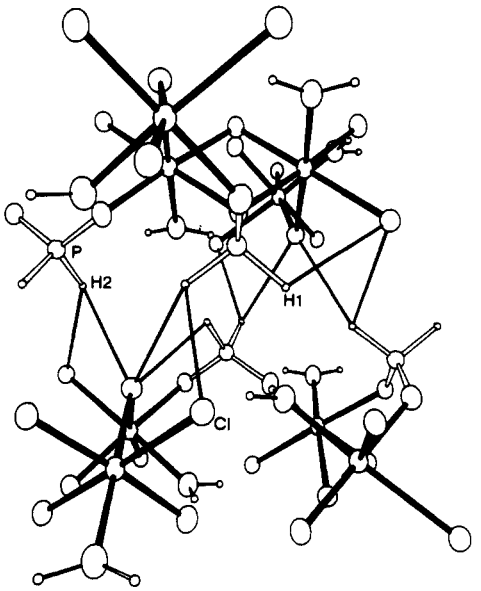

Figure 6. Representation of the possible interlayer hydrogen-bonding network in $NiCl(H_2PO_2)\cdot H_2O$.

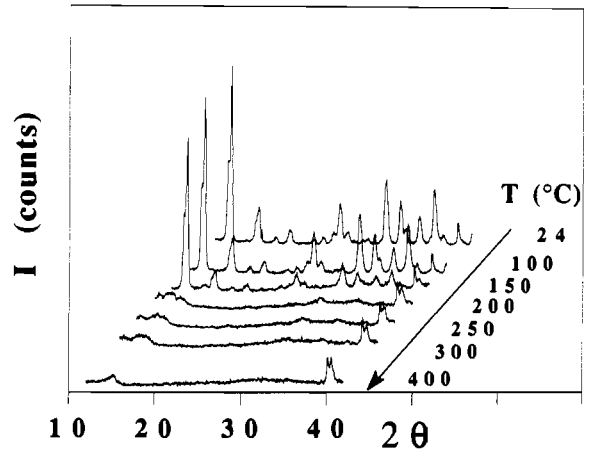

Figure 7. X-ray thermodiffractometry of $NiCl(H_2PO_2)\cdot H_2O$.

and play a bridging role throughout the structure comparable to that played by the hydroxo groups in the highly condensed materials obtained at higher pH values.[7,8]

A decrease in structural dimensionality due to lowering the number of donor oxygen atoms in pseudotetrahedral anions is not a universal feature. There are other factors that can affect the connectivity of the cations, for example, the presence of other coordinating anions. In addition, the different bridging modes that pseudotetrahedral species can adopt can give structures varying from 3D ($Mn(H_2PO_2)_2\cdot H_2O$[23]) to 1D ($VO(H_2PO_2)_2\cdot H_2O$[24]) with the same anion. The structure of the nickel phosphite $Ni(HPO_3)\cdot H_2O$ is built up from isolated layers, giving rise to a 2D system. The hypophosphite, $NiCl(H_2PO_2)\cdot H_2O$, might be expected to have a lower dimensionality, but the contribution of Cl^- anions to the connectivity of the octahedra also results in a 2D structure.

Crystal Structure of 1. Shown in Figure 3 are two different projections of the lamellar structure of **1**. The layers are formed by zigzag chains of edge-sharing octahedra (cis-$^1_\infty[Ni_2O_8]$ chains in the nomenclature proposed by Moore and Hawthorne[25]) running along the a direction, linked into sheets through P(2)-phosphite tetrahedra. This description is supported by the existence of two short Ni(1)–Ni(2) distances (3.04(1) and 3.09(1) Å) within the chains and a relatively large Ni(1)–N(2) separation (3.566(4) Å) between atoms of different chains. P(1)-phosphite groups connect nickel cations inside the chains only by means of two oxygen atoms; the third one remains uncoordinated and should be hydrogen-bonded to water molecules of adjacent layers, as occurs in the cobalt analogue.[11]

The crystallographically distinct nickel atoms Ni(1) and Ni(2) have very similar chemical environments, being surrounded by six oxygen atoms in an irregular octahedral coordination. A rough estimate of the cationic distortion is furnished by the equation $[\Delta = (1/6)\sum((R_i - R)/R)^2]$,[26] R_i being the individual bond length and R the average bond length. The calculated values,

Table VII. Bond Valence Analysis for $NiCl(H_2PO_2)\cdot H_2O$

	Co	H[a]	P	Σ
O(3)	0.37(2)		1.27(2)	1.84(4)
		0.19(H(3))[b]		2.03(4)[c]
O(1)	0.34(2)		1.24(2)	
	0.30(2)			1.88(6)
O(2)	0.35(2)	0.88 (H(3))		
		0.93(H(4))		2.16(3)
		0.08(H(1))[d]		2.24(3)[c]
Cl	0.27(2)			
	0.26(2)			0.53(4)
Σ	1.89(12)		2.51(4)	
	Ni	**H[a]**	**P**	**Σ**
O(3)	0.35(3)		1.40(4)	1.74(7)
		0.19 (H(3))[b]		1.94(7)[c]
O(1)	0.32(3)		1.19(2)	
	0.28(3)			1.78(8)
O(2)	0.27(3)	0.88 (H(3))		
		0.91 (H(4))		2.06(3)
		0.08 (H(1))[d]		2.15(3)[c]
Cl	0.31(2)			
	0.28(2)			0.59(4)
Σ	1.81(16)		2.58(6)	

[a] The bond valence calculations of the hydrogen bonds have been made with the Zachariasen law.[33] [b] Valences corresponding to the intralayer hydrogen bonds. [c] Valences corresponding to the interlayer hydrogen bonds. [d] Total valence taking into account the hydrogen bonds.

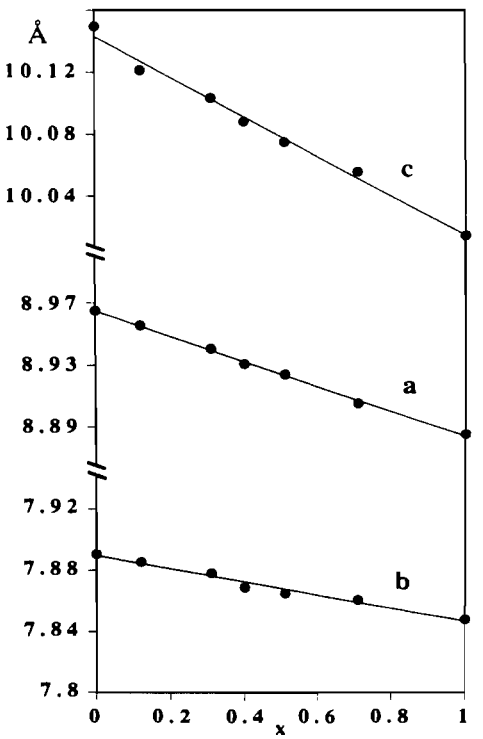

Figure 8. Cell parameters in the evolution of the $Co_{1-x}Ni_x(HPO_3)\cdot H_2O$ solid solution vs the nickel content (x).

(23) Marcos, M. D.; Amorós, P.; Sapiña, F.; Beltrán, D. *J. Alloys Comp.* **1992**, *188*, 133.
(24) Le Bail, A.; Marcos, M. D.; Amorós, P. *Inorg. Chem.*, submitted for publication.
(25) Moore, P. B. *Second International Congress on Phosphorus* Compounds *Proceedings*, April 21–25, Boston, MA, 1980. Institut Mondial du Phosphate, 105. Hawthorne, F. C. *Am. Mineral.* **1985**, *70*, 455.

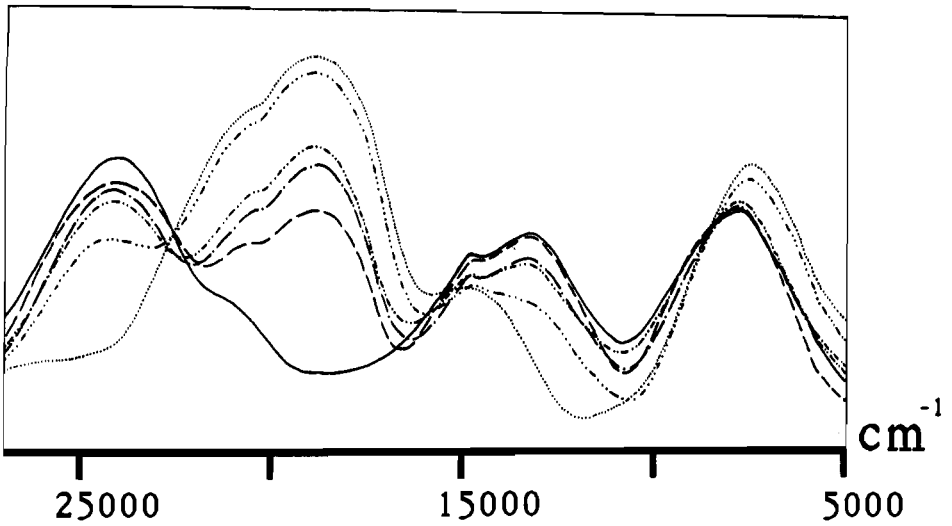

Figure 9. Visible diffuse reflectance spectra of the $Co_{1-x}Ni_x(HPO_3)\cdot H_2O$ solid solution members: (a) $x = 0.0$; (b) $x = 0.12$; (c) $x = 0.31$; (d) $x = 0.40$; (e) $x = 0.51$; (f) $x = 1.0$.

Table VIII. Visible Spectral Data and Crystal Field Parameters for $M(HPO_3)\cdot H_2O$ (M = Co, Ni)

$Ni(HPO_3)\cdot H_2O$		
position (cm^{-1})	intens (%)	assgnt
7 800	25	ν_1
13 100	20	ν_2
14 800	18	$^3A_{2g} \rightarrow {}^1E_g$
20 600	10	$^3A_{2g} \rightarrow {}^1A_1$
24 300	28	ν_3
Crystal Field Parameters		
$\Delta_0 = 7800\ cm^{-1}$	$B' = 940\ cm^{-1}$	$\beta = 0.90$
$Co(HPO_3)(H_2O)$		
position (cm^{-1})	intens (%)	assignt
7500	38	ν_1
14800	22	ν_2
18900	52	ν_3
21000	40	$^4T_{2g} \rightarrow {}^2A_{2g}$
Crystal Field Parameters		
$\Delta_0 = 8465\ cm^{-1}$	$B' = 838\ cm^{-1}$	$\beta = 0.86$

$\Delta(Ni(1)) = 0.018\%$ and $\Delta(Ni(2) = 0.038\%$, are significantly lower than those found in the case of the isostructural cobalt derivative ($\Delta(Co(1)) = 0.032\%$, $\Delta(Co(2)) = 0.083\%$), a result which is in accord with the Jahn–Teller activity of Co^{2+}.

The two water molecules (OW(1), OW(2)) are coordinated to nickel atoms (Table III) and participate in the interlayer hydrogen-bonding network. Both thermal analysis and X-ray thermodiffractometry show that the material is stable up to 230 °C and water evolution is observed between 230 and 350 °C, leading to an amorphous solid (Figure 4). A bond valence analysis of this structure[27] allows us to confirm the presence of hydrogen-bonding interactions. As shown in Table VI, neglecting OW(1) and OW(2) (whose seemingly very low valences are mainly due to the fact that O–H bonds have not been included in the calculations), the only oxygen atom which would have a deficient valence is O(2). This deficit can be attributed to the existence of (noncomputed) strong hydrogen-bonding interactions involving this oxygen atom and the protons of the coordinated water molecules.

Crystal Structure of 2. A polyhedral representation (STRUPLO[28]) of **2** is shown in Figure 5. In this compound, the nickel cations present a distorted octahedral coordination, $NiCl_2O_3(H_2O)$. The average distortion values calculated as above, $\Delta(Ni) = 0.65\%$ and $\Delta(Co) = 0.77\%$, again reflect the Jahn–Teller activity of Co^{2+}. Dimers of edge-sharing octahedra are linked to four other dimers through chloride bridges, resulting in layers in the *ac* plane. The interlayer interactions are due to van der Waals forces and very weak hydrogen bonds. There are no close contacts between layers: the shortest distance between them is 2.6 Å (Table V). Although the nonprotonic character of the hydrogen atoms of the hypophosphite anions does not usually lead to hydrogen bonding, the distances (Table V) indicate that very weak interlayer hydrogen bonding occurs (P–H(1)···O(2) and P–H(2)···Cl). A view of the possible interlayer hydrogen bonds is shown in Figure 6.

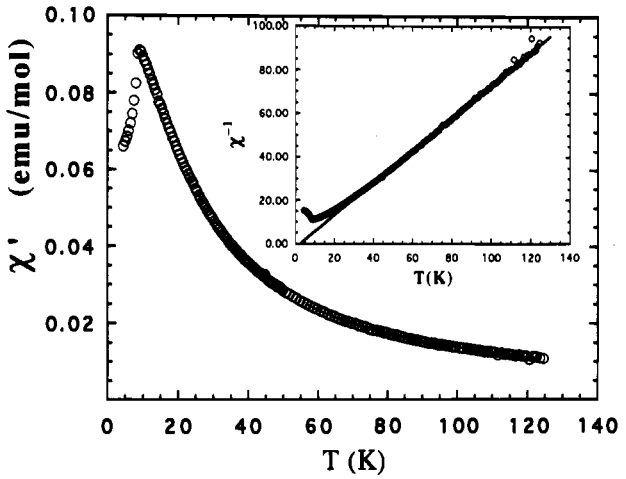

Figure 10. Thermal evolution of the magnetic susceptibility (χ_m') of $Ni(HPO_3)\cdot H_2O$. In the inset we have represented the variation of the inverse molar susceptibility vs temperature.

The water molecule in **2** is coordinated to the nickel atom and only forms intralayer hydrogen bonds to the oxygen atom of the hypophosphite anion (O(2)–H(3)···O(3); 1.82(9) Å) and the chloride anion (O(2)–H(4)···Cl; 2.36(6) Å). This is consistent with the high temperature of its evolution, 150 °C, observed in the TGA experiments. In addition, an X-ray diffractometric study (Figure 7) leads to the following results: (i) $NiCl(H_2PO_2)\cdot H_2O$ is stable in air up to ca. 100 °C. The position and intensity of the 010 peak are unchanged (13.65° 2θ), and the width at half-height of this peak also remains practically constant. (ii) Between 100 and 200 °C dehydration occurs. The intensity of the 010 peak decreases slowly from 100 to 150 °C and then falls sharply and disappears at ca. 200 °C, at which temperature an amorphous material is formed.

(26) Shannon, R. D. *Acta Crystallogr., A* **1976**, *32*, 751.
(27) Brese, N. E.; O'Keeffe, M. *Acta Crystallogr., B* **1991**, *47*, 192.
(28) Fischer, R. X. *J. Appl. Crystallogr.* **1985**, *18*, 258.
(29) Lovejoy, R. W.; Wagner, E. L. *J. Phys. Chem.* **1964**, *68*, 544.
(30) Tsuboi, M. *J. Am. Chem. Soc.* **1957**, *79*, 1351.

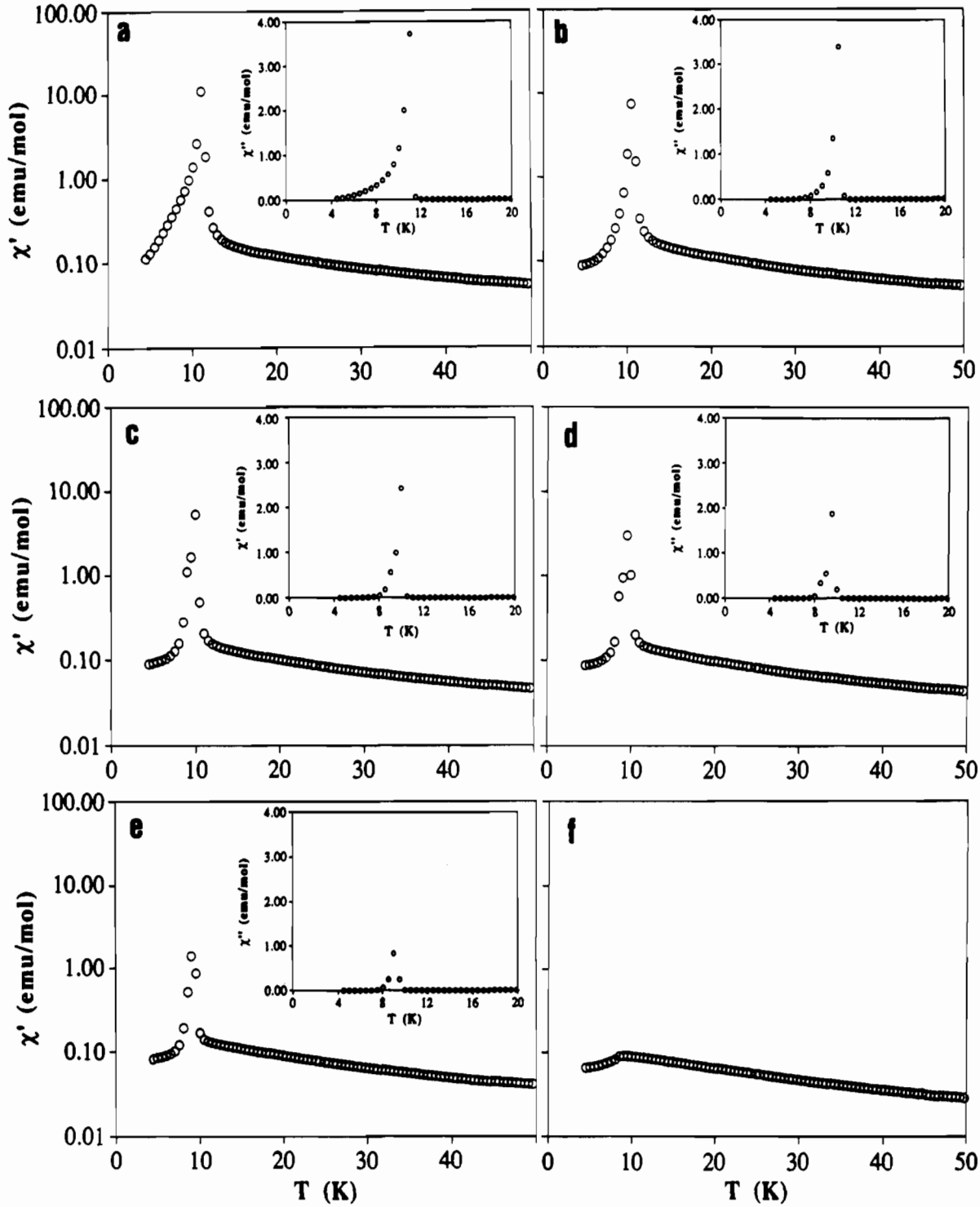

Figure 11. χ'_m and χ_m'' vs T plots for the different members of the $Co_{1-x}Ni_x(HPO_3)\cdot H_2O$ solid solution series: (a) $x = 0.0$; (b) $x = 0.12$; (c) $x = 0.31$; (d) $x = 0.40$; (e) $x = 0.51$; (f) $x = 1.0$.

A bond valence analysis[27] of $MCl(H_2PO_2)\cdot H_2O$ compounds (M = Co, Ni) (Table VII) has shown a deficient valence for both metals: 1.81(16) vu for nickel and 1.89(12) vu for cobalt. Also, in both cases, the chloride valence is much lower than the expected one. Although the hydrogen bonds have not been included in the calculations, this deficit is too large to be assigned to these interactions. The parameters given by Brese and O'Keeffe[27] for the M–Cl bonds may be based on tetrahedral M–Cl distances which are inadequate for our compounds. Using the bond valence law, we find a more adequate M–Cl parameter to be (R_0(M–Cl) = 2.09), a value slightly larger than those proposed in ref 27 for cobalt (2.01 Å) and nickel (2.02 Å) metal–chloride bonds. The bond valences of cobalt and nickel atoms, taking this new parameter into account, are 2.01(12) and 1.94(18) vu, respectively. Notwithstanding, the valences of the Cl atoms remain low in both compounds (0.65(2) and 0.72(3) vu for cobalt and nickel derivatives, respectively), as the contributions from intra- and interlayer hydrogen bonds are not included.

The cell parameters of **2**, in comparison with those of its cobalt analog, decrease as the cationic radius decreases, but variations in the a and c parameters (1.6% and 0.8%, respectively) are larger than that in b (0.16%). As can be expected, larger dimensional changes are found in the ac plane, which corresponds to the layer propagation direction.

Study of the $Ni_xCo_{1-x}(HPO_3)\cdot H_2O$ Solid Solutions. Variation of the cell parameters and volume with the nickel mole fraction (x) is presented in Figure 8.

The lattice parameters of solid solution series usually show a

small variation with composition. If the composition dependence is linear, then Vegard's law is said to be obeyed. Deviations from this law occur in metallic solid solutions, but for nonmetallic ones deviations are much less common. In the latter case, deviations are related to incipient immiscibility and/or cationic ordering in the solid solutions. In $Ni_xCo_{1-x}(HPO_3)\cdot H_2O$ solid solutions, the changes in the cell dimensions can be linearly correlated with the nickel mole fraction, x. Larger dimensional changes are found in the a and c axes. As discussed above, the minor variations observed in the [010] direction are due to the insensitivity of the hydrogen-bonding network, which governs the stacking of the layers, to the variation of the cation size.

These solid solutions have also been studied by diffuse reflectance spectroscopy. In Figure 9 the visible spectra of these materials are shown. The absorption maxima positions and their assignments for the cobalt and nickel compounds are shown in Table VIII. The crystal field parameters obtained from these assignments are characteristic of slightly distorted octahedral environments, for both the nickel and cobalt compounds. In no case is it possible to distinguish between the two crystallographic sites of the metallic atoms. A regular evolution of the intensity of the bands is observed when the nickel/cobalt molar ratio increases. Hence, we can summarize that the two phosphites are miscible over the whole concentration range and that no cationic ordering occurs.

Magnetic Behavior. The magnetic behavior of $Ni(HPO_3)\cdot H_2O$ is illustrated in Figure 10 through a plot of the in-phase molar susceptibility χ' vs T. In the inset, we have represented the temperature dependence of the inverse of the molar susceptibility, χ'^{-1}. Within experimental error, the out-of-phase component of the *ac* susceptibility χ'' remains zero for this compound.

The susceptibility increases on cooling, reaching a maximum at $T_{max} = 9.8 \pm 0.2$ K ($\chi_{max} = 0.092$ emu mol^{-1}), and then decreases. As observed in Figure 10, the susceptibility data between 50 and 130 K follow the Curie–Weiss law. The value of the Curie constant obtained from this fit is very close to that expected for a nickel(II) ion ($C = 1.315$ emu K mol^{-1}), from which a value of the effective moment per nickel(II) ion of 3.24 μ_B could be obtained. The value of the Curie–Weiss temperature, $\Theta = 4.22$ K, can be attributed to the presence of predominantly ferromagnetic interactions. However, at low temperatures, the susceptibility deviates from Curie–Weiss behavior, due to antiferromagnetic ordering.

Magnetic interactions in this compound are mediated by different exchange pathways between nickel(II) ions, giving rise to three inequivalent exchange integrals. J_x and J_y describe the intralayer interactions. As has been previously stated, each layer could be described as cis-sharing-edge octahedra chains that join together through complicated phosphite bridges. Hence, each nickel(II) ion shares one edge (bis(μ-(O)-phosphite)bridge) with two other nickel(II) ions inside the chains and also one corner with another nickel ion belonging to a neighboring chain. In addition to these connections, there are several μ-(O,O')-phosphite bridges, both inside the chains and among them, that complete the connectivity in the layers. J_z describes the interlayer interaction between nickel(II) ions. This interaction is only sustained by hydrogen bonds, and so, J_z is expected to be the weakest of the three different interactions.

A magnetic phase transition from the paramagnetic to a 3D antiferromagnetic ordered state may be inferred from the susceptibility curve, and the critical temperature for this transition is estimated to be $T_c = 8.1 \pm 0.4$ K, from the maximum in $d\chi/dT$.[31] This is consistent with preliminary low-temperature powder neutron diffraction experiments on this compound,[32] which show the appearance of additional diffraction peaks at around 8 K.

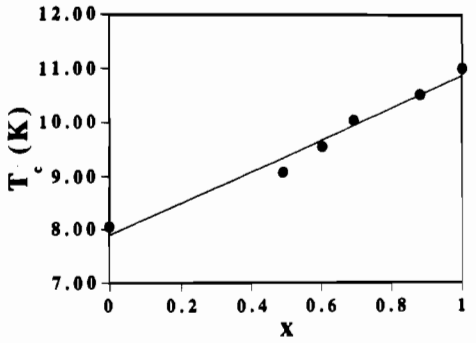

Figure 12. Variation of the critical temperature with the cobalt content (X equivalent to $(1 - x)$ in $Co_{1-x}Ni_x(HPO_3)\cdot H_2O$).

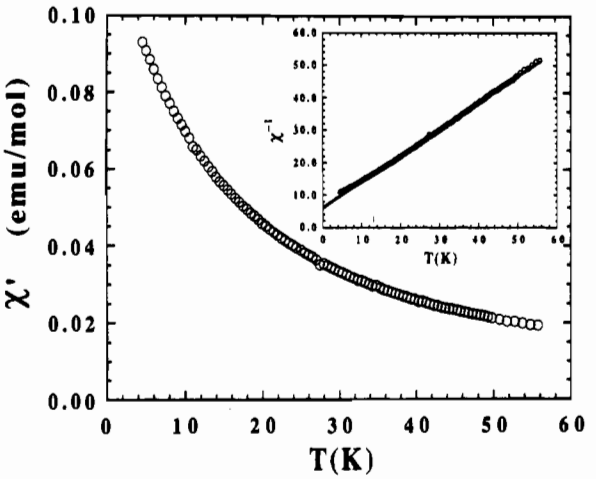

Figure 13. Thermal evolution of the magnetic susceptibility (χ'_m) of $NiCl(H_2PO_2)\cdot H_2O$. In the inset we have represented the variation of the inverse molar susceptibility vs temperature.

The magnetic behavior of the solid solution, $Ni_xCo_{1-x}(HPO_3)\cdot H_2O$, has also been studied. The thermal variation of the in-phase component of the *ac* susceptibilities, χ', of these solids are shown in Figure 11, using the same logarithmic scale in order to facilitate the comparison. The magnetic behavior of $Co(HPO_3)\cdot H_2O$ has been previously reported;[11] it behaves as a weak ferromagnet with critical temperature $T_c = 10.8 \pm 0.1$ K. Except for the $x = 1$ compound, sharp peaks are observed at T_c. Sharp peaks are also observed in the out-of-phase component of the *ac* susceptibilities, χ'', indicating that all the cobalt containing compounds behave as weak ferromagnets, as the pure cobalt compound does. The χ' and χ'' values at the maximum decrease regularly with the molar cobalt concentration, as well as the critical temperature T_c (Figure 12). These results are also consistent with the low-temperature powder neutron diffraction patterns of the two limiting compositions, $Co(HPO_3)\cdot H_2O$ and $Ni(HPO_3)\cdot H_2O$. Additional magnetic peaks appear below 11 and 8 K, respectively, at the same (hkl) values and with similar relative intensities, which indicates that the same basic spin structure (based on an antiferromagnetic mode) is established in both compounds. The regular variation of $(\chi')_{max}$, $(\chi'')_{max}$, and T_c also supports the previous conclusion of a random cation distribution in the metallic lattice.

The temperature dependence of the in-phase molar susceptibility χ' of $NiCl(H_2PO_2)\cdot H_2O$, measured in the temperature range 4.5–60 K, is shown in Figure 13. The susceptibility continuously decreases upon cooling, without any special features. As observed in the inset of Figure 13, the magnetic susceptibility follows the Curie–Weiss law above 15 K, with $\Theta = -1.0$ K and $C = 1.232$ emu K mol^{-1}, from which a value of 3.14 μ_B for the effective moment per nickel(II) ion could be obtained. The value of the Curie–Weiss temperature is indicative of the presence of dominant antiferromagnetic interactions. No evidence of a magnetic phase transition to a long-range ordered magnetic state

(31) Carlin, R. L. *Magnetochemistry*; Springer: Berlin/Heidelberg, 1986; p 122.
(32) Marcos, M. D.; et al. Unpublished results.
(33) Zachariasen, W. H. *J. Less Common Met.* **1978**, *62*, 1.

above 4.5 K is observed, in contrast with the behavior of the isostructural compound $CoCl(H_2PO_2)\cdot H_2O$, which behaves as a weak ferromagnet with critical temperature $T_c = 8.4 \pm 0.1$ K.[11]

Concluding Remarks

Phosphite and hypophosphite compounds have not been widely studied and also, in most cases, have not been considered in systematic classifications of mineral structures. Moore and Hawthorne[25] have proposed a classification of phosphate, sulfate, arsenate, vanadate, and silicate materials attending to the morphology of the metallic clusters and the structural characteristics that are generated from its spatial repetition.

In this work, we have presented the syntheses and structures of two new layered compounds. In both cases, the layers can be viewed without the pseudotetrahedral species and, in this way, both compounds may be easily included in the Hawthorne classification. Hence, $NiCl(H_2PO_2)\cdot H_2O$ can be thought as formed by *cis*-$^1_\infty[M_2\Phi_9]$ interconnected chains that run in the 001 direction or, in an alternative way, as *trans*-$^1_\infty[M_2\Phi_9]$ interconnected chains along the 101 direction. On the other hand, we have to consider a new chain type to describe the layers in the $Ni(HPO_3)\cdot H_2O$: it is written as *cis*-$^1_\infty[M_2\Phi_7]$ running along the 100 direction. In their respective views (Figures 3 and 5), the octahedra involved in the chain motif have been strongly shaded.

As occurs for phosphate and other pseudotetrahedral anions, the structural diversity of oxophosphorus derivatives allows us to search for correlations leading to the rationalization of their magnetic properties. Initially, it may be expected that the activity of μ-(O) bridges in the transmission of exchange interactions should be more relevant than that of the μ-(O,O′) ones. However, this activity will depend to a great extent on their topology and relative orientation of magnetic orbitals. In order to clarify these aspects, more detailed studies of magnetic properties, including solid-state ^{31}P NMR and neutron powder diffraction experiments, are needed.

Acknowledgment. We thank the Institució Valènciana d'Estudis i Investigació (IVEI) and the DGICYT of the Spanish Ministerio de Educación y Ciencia (Grant PB91-0459) for financial support of this work. M.D.M. thanks the Spanish Ministerio de Educación y Ciencia for an FPI fellowship.